Magnetic Resonance in Medicine 43:52–61 (2000)

Histogram-Based Characterization of Healthy and Ischemic Brain Tissues Using Multiparametric MR Imaging Including Apparent Diffusion Coefficient Maps and Relaxometry

J. Bernarding,[1,2]* J. Braun,[1] J. Hohmann,[2] U. Mansmann,[1] M. Hoehn-Berlage,[4] C. Stapf,[3] K.-J. Wolf,[2] and T. Tolxdorff[1]

Decreased, renormalized, or increased values of the calculated apparent diffusion coefficient (ADC) are observed in stroke models. A quantitative description of corresponding tissue states using ADC values may be extended to include true relaxation times. A histogram-based segmentation is well suited for characterizing tissues according to specific parameter combinations irrespective of the heterogeneity found for human healthy and ischemic brain tissues. In a new approach, navigated diffusion-weighted images and ADC maps were incorporated into voxel-based parameter sets of relaxation times (T_1, T_2), and T_1- or T_2-weighted images, followed by a supervised histogram-based analysis. Healthy tissues were segmented by incorporating T_1 relaxation into the data set, ischemic regions by combining T_2- or diffusion-weighted images with ADC maps. Mean values of healthy and pathologic tissues were determined, spatial distributions of the parameter vectors were visualized using color-encoded overlays. One to six days after stroke, ischemic regions exhibited reduced relative mean ADC values. Magn Reson Med 43:52–61, 2000. © **2000 Wiley-Liss, Inc.**

Key words: diffusion-weighted imaging; tissue characterization; multimodal imaging; stroke; segmentation

Diffusion-weighted images (DWI) display ischemic regions within minutes after the onset of ischemia as relative hyperintense regions (1), caused by the reduction in the apparent diffusion coefficient (ADC). The ADC may normalize after reperfusion and increase to supranormal values in later stages (2–4). There is consensus that the ADC as a quantitative measure for the mobility of water protons may allow the comparison of pathophysiologic processes in humans and stroke models. However, there is still some debate about how to quantify ADC values of ischemic human tissues with respect to unaffected tissues, as well as the predictive value of ADC changes for recovery or necrosis of affected tissue (5–7). Several factors impede the determination of the ADC values and their spatial distribution for human brain tissues. The extreme motion sensitivity of diffusion-weighted imaging requires ultrafast imaging (8) or navigator echo methods (4,9), each of which has different advantages, drawbacks, and technical limitations (3,10). But given healthy volunteers and the elimination of motion artifacts, the complex human brain anatomy still results in a broader distribution of ADC values than that obtained in stroke models where the middle cerebral artery (MCA) is occluded, often leading to a large connected ischemic area with strongly decreased ADC values. By contrast, ischemic tissues in humans may exhibit irregular or disconnected regions, a high degree of heterogeneity with acute and chronic lesions as well as hemorrhagic parts, and increased partial volume effects if located near the strongly folded human brain surface. Generally, pathologic regions are segmented within a parameter image, and the mean value of the region of interest (ROI) is determined. Relative changes are determined as the ratio to the mean parameter value of a similar ROI in an unaffected region (most often in the contralateral hemisphere). This yields reliable results for regions with few spatial heterogeneities. However, a histogram-based data analysis may be better suited for segmenting tissues with similar physiologic characteristics in irregularly shaped, disconnected, or heterogeneous regions. This approach may also be easily extended to a multidimensional data set, allowing a simultaneous description of the combined parameters: different tissue classes may cluster into separable histogram regions according to their characteristic parameter distributions. The histogram analysis may also clarify whether certain parameter combinations can be correlated to different substructures within ischemic regions (11–14), as proposed by the concept of tissue signatures (5). The most important task is to predict which tissue will necrotize and to determine the zones of tissue at risk that might recover (5,14,15).

To investigate whether tissues may be characterized by quantitative parameters, we incorporated for the first time ADC maps and true relaxation times into a multi-spectral parameter set of navigated DWI and standard clinical images. Histogram-based methods using spin density, true T_1 and T_2 (or corresponding relaxation rates) were applied to analyze healthy brain tissues and experimental tumors (16–21). Besides preliminary results published in abstract form (22), a histogram-based characterization of human ischemic brain tissues using ADC maps, T_2- and diffusion-weighted images has been reported only by Welch and

[1]Department of Medical Informatics, University Hospital Benjamin Franklin, Free University of Berlin, Berlin, Germany.

[2]Department of Radiology and Nuclear Medicine, University Hospital Benjamin Franklin, Free University of Berlin, Berlin, Germany.

[3]Department of Neurology (Stroke Unit), University Hospital Benjamin Franklin, Free University of Berlin, Berlin, Germany.

[4]Max Planck Institute for Neurological Research, Cologne, Germany.

Grant sponsor: Deutsche Forschungsgemeinschaft; Grant number: To108/3–2.

*Correspondence to: Johannes Bernarding, Ph.D., M.D., Department of Medical Informatics, University Hospital Benjamin Franklin, Free University of Berlin, Hindenburgdamm 30, D-12200 Berlin, Germany.
E-mail: bernarding@ukbf.fu-berlin.de

Received 2 April 1998; revised 2 September 1999; accepted 3 September 1999.

others (5,23). However, they analyzed the histogram with a different strategy than the one presented in this work (5).

Since the data set included other spin-echo-based images, we had to use navigated spin-echo-based DWI (9,24), which resulted in geometrically undistorted images with a higher spatial resolution compared to echo planar imaging (EPI). Parameter distributions of a segmented histogram region were color-encoded and superposed onto the corresponding parameter images, displaying both physiologic and anatomical information simultaneously. A multiparametric data set of unaffected tissue classes served as reference data. Different parameter combinations were examined with regard to the minimal number of parameters needed to reliably segment healthy and pathologic tissue classes. Healthy volunteers and patients were examined. Two cases will illustrate in detail typical problems associated with the analysis of human ischemic regions and the results obtained by the proposed method.

METHODS

Examination

Seventeen healthy volunteers (10 male, 7 female, 24–57 years, mean 33.7 years), and 10 patients (7 male, 3 female, 35–64 years, mean 55.7 years) were examined after providing written consent, in accordance with the board of ethics. Patients were admitted to the neurological department of the hospital because of acute cerebral ischemia. Three patients in poor condition were examined without determining exact relaxation times. One patient with a transient neurological deficit did not show abnormalities in T_1-weighted (T_2w), T_2-weighted (T_2w), or DWI. Eight patients exhibited hyperintense regions in DWI and T_2w images, whereas one patient (examined 4 months after ischemia) showed hyperintense signals in the T_2w image and corresponding hypointense signals in the DWI. Healthy and affected tissues were identified by a radiologist according to their specific signal behavior in the different images. Diagnoses were ascertained in a clinical follow-up.

MR Imaging and Data Postprocessing

Two spin-echo pulse sequences were implemented on a standard clinical MR scanner (1.5 T, Magnetom Vision, Siemens). A navigated diffusion-sensitive double-spin-echo sequence was used for DWI (9,24,25) with $TE_{(image\ echo)} = 76$ msec, $TE_{(navigator\ echo)} = 95$ msec. Diffusion-encoding gradients were applied along the phase-encoding direction (short axis of the head). Diffusion weighting with variable *b*-values (0–529 sec/mm^2) was achieved with amplitudes of the diffusion gradients (G_D) between 0 and 20 mT/m according to

$$b = \gamma^2 G_D^2 \delta^2 (\Delta - \delta/3) \qquad [1]$$

with a gradient duration of $\delta = 28$ msec, a difference between the leading edges of the gradient lobes $\Delta = 35$ msec, and γ as the gyromagnetic ratio of the proton. Seven slices with a matrix size of 128*256 were acquired using pulse-triggered data acquisition (TR = 850 msec, trigger delay 100–150 msec, effective TR about 1500 msec). Motion artifacts were corrected in the frequency domain analogous to (9,24). In a few cases this algorithm did not correct motion-induced artifacts in localized regions. The original navigator phases of these regions were then interactively replaced by navigator phases interpolated from adjacent nondistorted regions. A second navigator method, using phase correction in the time domain, led to insufficient results in patient examinations (26). All voxels above an automatically determined noise level were selected for the ADC calculation by applying a linear least squares fitting routine to the logarithm of the signal intensity as a function of the *b*-values (0, 132, 259, 428, 529 sec/mm^2). The mismatch of voxels caused by minor patient movements between measurement cycles (most prone at border structures) was reduced by applying a motion-correcting software (27). Data were post-processed on the scanner console with a self-developed software system. Corrected images and ADC maps were stored in the database system of the vendor, allowing immediate data evaluation by neuroradiologists. ADC calculation took about 3 min for 7 slices, 5 *b*-factors, and a 128*256 matrix size.

Exact longitudinal and transversal relaxation times, initial magnetization, and relative proton densities were determined simultaneously using a special multi-echo sequence followed by a nonlinear data analysis similar to (16). Two pulse trains (28 and 4 echoes with a time spacing $\Delta TE = 22.5$ msec, separated by a fixed TR of 500 msec) were recorded. Repetition time varied between 2200 and 3000 msec. Only voxels above an automatically determined noise level were selected for further analysis (16). T_1 relaxation time and relative spin density were calculated from the first 4 echoes of each echo train according to (28). The first 28 echoes were used for the nonlinear multi-exponential analysis of the T_2 relaxation time and the initial magnetization (16,29). All data were fitted with a mono-exponential curve. Voxels with a χ^2 statistic greater than χ^2_ν, $1 - \alpha$ (ν = degrees of freedom, $\alpha = 0.05$) were additionally fitted by a bi-exponential curve. To assess the improved fit, an F-test on level $\alpha = 0.05$ was performed. Adjacent voxels were compared to estimate whether bi-exponential T_2 behavior was caused by partial volume effects or by intrinsic tissue characteristics (16,17,21). Data were analyzed using a two-tailed paired Student's *t*-test. *P*-values below 0.05 were considered to be significant.

Data Analysis

The supervised histogram-based analysis was performed on a DEC Alpha 300, requiring about 6 min for data transfer, image registration, parameter evaluation, and histogram generation. Multidimensional histograms were constructed by combining 1D histograms of selected parameter subsets (30). Histogram segmentation was performed using rectangular ROIs. In 2D histograms, arbitrarily shaped ROIs could also be used. To analyze parameters that were unequally distributed within their ranges (e.g., T_2), the histogram axes could be scaled logarithmically or inversely. Contrast was optimized by freely adjusting the window size and the center of both the histogram and the parameter images. In a given histogram (e.g., T_1-T_2), voxels within the selected ranges of an ROI were color-encoded according to the parameter range (e.g., T_1) and then superposed onto the original parameter images. The overlay color blue (or red) stood for the minimum (or maximum)

value of the selected parameter ranges. The original parameter image and color-encoded overlay could be displayed separately. To verify the histogram-based tissue segmentation, a control segmentation of regions that were hyperintense in the DWI (Table 1, patients 1 and 3–9) or in the T_2w image (patient 2) was performed by a second radiologist, who was blinded for the results of the histogram method. ROIs were subsequently transferred to other images (e.g., T_2w image or ADC map). Contralateral ROIs with similar shape and comparable location were selected and their mean parameter values were determined. Ratios of mean values of ischemic to contralateral unaffected tissues were determined. Histogram cells corresponding to the parameter combinations of the voxels within the selected ROI of the image were color-encoded and superposed onto the original histogram. For a definition of false-positive voxels, see Table 1.

Histogram and images could be zoomed to account for small or irregular structures. Number of segmented voxels, parameter ranges, mean values, standard deviations of segmented tissues, and their ratios to unaffected brain parenchyma were automatically calculated, displayed, and stored in a data base.

RESULTS

Nonischemic Tissue

Figure 1 displays original parameter images and ADC values of representative healthy brain tissues obtained by an interactive segmentation of true T_1, T_2, and ADC values. The spatial distribution of the ADC is visualized by using color-encoded overlays. Comparable segmentation results were obtained by analyzing different 2D histograms, given that arbitrarily shaped ROIs were used instead of rectangular ones: In a T_1-T_2 histogram, gray matter (GM), white matter (WM), cerebrospinal fluid (CSF), adipose tissue, and muscle could be segmented; a T_1-ADC histogram allowed the differentiation of GM, WM, and CSF. Muscle and adipose tissue could not be differentiated from each other but were clearly distinct from GM, WM, or CSF**.** In healthy volunteers a T_2-ADC histogram generally allowed only the differentiation between brain parenchyma (WM/GM), CSF, and muscle/adipose tissue (similar to the T_1-ADC histogram). The mean and standard deviation of the parameters were determined for the tissues of volunteers and the unaffected tissues of patients. Mean ADC values were 890 ± 215 μm^2/sec for GM, 810 ± 270 μm^2/sec for WM, and 3100 ± 660 μm^2/sec for CSF. In WM, the ADC values per voxel varied between 1500 μm^2/sec (parallel to the diffusion-weighting gradients) and 230 μm^2/sec (nerve fiber direction perpendicular to the gradients). The few voxels corresponding to adipose tissue and muscle exhibited widely scattered and nonseparable ADC values (780 ± 700 μm^2/sec).

Mean T_1 relaxation times were 1120 ± 120 msec for GM, 780 ± 89 msec for WM, 1715 ± 600 msec for CSF, 395 ± 81 msec for adipose tissue, and 1072 ± 290 msec for muscle. Mean T_2 relaxation times were 96 ± 8 msec for GM, 92 ± 8 msec for WM, and 50 ± 10 msec for muscle. Mean T_2 relaxation for adipose tissue was 111 ± 30 msec, which could be resolved into two decay components with mean values of 34 ± 8 msec and 165 ± 31 msec. Partial volume effects between brain parenchyma and CSF were resolved in surface-adjacent CSF parts, showing a bi-exponential T_2 relaxation with mean values of 79 ± 12 msec and 1052 ± 485 msec. Mono-exponential T_2 relaxation for CSF was 1458 ± 400 msec.

Table 1
Histogram- and Image-Based Analysis of Ischemic Tissues Using T_2- and Diffusion-Weighted Imaging*

Patient	Time after onset of ischemia	Relative size of ischemic regions		Relative mean signal intensity (SI)				Classification statistics						Performance
				T_2w SI		ADC		Histogram			Image			
		Histogram	Image	Histogram	Image	Histogram	Image	IA	IB	IC	IIA	IIB	IIC	
1	6 days	0.109	0.075	1.41	1.53	0.64	0.70	0.066	0.112	0.27	0.147	0.135	0.041	1a,b
2	4 mo	0.037	0.044	2.18	2.11	2.53	2.17	0	0.06	0.004	0.038	0.125	0.019	1a; 3a
3	16 days	0.108	0.082	1.75	1.63	1.55	1.61	0.061	0.132	0.172	0.058	0.141	0.05	1a,b,c; 3a
4	3 days	0.311	0.339	1.38	1.39	0.67	0.66	0.008	0.002	0.053	0.022	0.039	0.013	1b
5	3 days	0.126	0.155	1.48	1.48	0.91	0.95	0	0	0.025	0.066	0.035	0.01	0
6	6 days	0.004	0.003	1.58	1.51	0.68	0.68	0.077	0	0.077	0.051	0.152	0.017	2
7	1 day	0.002	0.002	1.30	1.22	0.55	0.62	0.133	0	0.167	0.181	0	0.091	3b
8	2 days	0.293	0.312	1.39	1.40	0.59	0.60	0.008	0.006	0.062	0.019	0.028	0.028	0
9	6 days	0.030	0.039	1.47	1.39	0.85	0.80	0.015	0	0.006	0.003	0.092	0	(1d*)
		0.014	0.011	1.15	1.12	0.37	0.38	0.023	0	0.39	0.071	0.165	0.071	2; 3b

*Results of patients diagnosed with cerebral ischemia. Patient 9 (case 2) with a progressive stroke exhibited lesions with different T_2w-ADC combinations (see Fig. 5). One patient with a transient neurological deficit did not exhibit abnormalities in the DWI (data not shown). Sizes and SI are displayed as the ratio of the parameters of ischemic tissue relative to the parameters of unaffected tissue (see text for details). The classification statistics shows the false-positive (FVR) voxels for both methods as ratios of the number of misclassified voxels to the number of ischemic voxels. FVR of the histogram-based method: Voxels localized within the histogram ROI of ischemic tissues but projected within the image onto (IA) unaffected brain parenchyma, (IB) regions with increased partial volume effects, or (IC) other non-ischemic tissues (mostly muscle or adipose tissue). FVR of the image-based method: Parameter combinations of voxels localized in the image within the segmented ischemic tissues but projected onto histogram regions with characteristics of (IIA) unaffected parenchyma, (IIB) partial volume effects between ischemic tissues and parenchyma or CSF, or (IIC) with ADC values below the lower border of the histogram ROI of unaffected parenchyma but outside the histogram ROI of ischemic tissues. The last column summarizes the performance of the segmentation procedures: (1) histogram-based segmentation was faster than image-based ROI segmentation due to (1a) increased partial volume effects, (1b) heterogeneous, (1c) irregular or (1d) multiple ischemic regions. (2) Segmentation in the image was faster than histogram-based segmentation. (3) The contralateral ROI was not reliable due to (3a) partial volume effects and (3b) strongly varying ADC values (e.g., old lesions or anisotropy effects). (0) Both methods worked equally well. (*): the complete segmentation of all lesions of patient 9 was faster in the histogram.

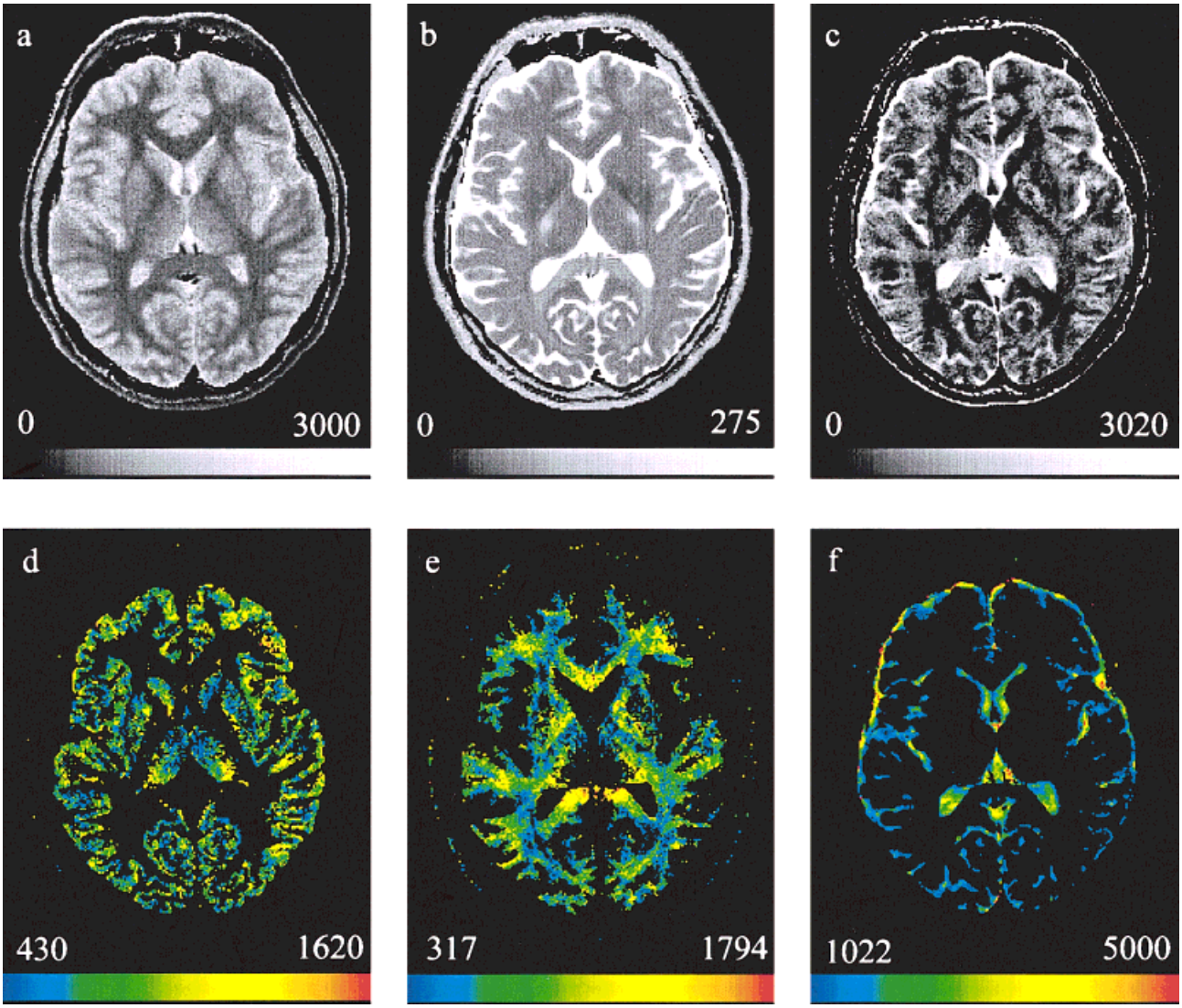

FIG. 1. Selected results of an interactive 3D segmentation of the main cerebral structures using quantitative T_1 relaxation, T_2 relaxation, and ADC values. Upper row: Original parameter images of T_1 (**a**), T_2 (**b**), and ADC (**c**). The gray-value encoding corresponds to the gray-scale bar at the bottom. To enhance contrast, the window of the T_2 values is set from 0–275 msec; T_2 values between 275 msec and 2500 msec are encoded white. The broad range of T_2 values of the CSF is due to partial volume effects. Lower row: ADC values for gray matter (GM) (**d**), white matter (WM) (**e**), and cerebrospinal fluid (CSF) (**f**). The color bar shows the upper and lower parameter limits. The different ADC values of the WM tracts, parallel and orthogonal to the diffusion gradient (applied parallel to the short axis of the head), can be clearly recognized. The overlays are shown without the underlying parameter image to control the quality of the segmentation result. Not shown are the segmented overlays for T_1 of GM (segmentation range 930–1387 msec), WM (s.r. 581–989 msec), and CSF (s.r. 753–3000 msec), T_2 of GM (s.r. 76–145 msec), WM (s.r. 67–141 msec), and CSF (s.r. 149–2500 msec).

Ischemic Tissue

Various parameter combinations were examined with respect to the minimal number of input parameters necessary to differentiate unaffected from ischemic tissues as well as to characterize substructures: 1) The ADC distribution of ischemic regions with increased T_2 values could be determined by analyzing the T_2-weighted-ADC (T_2w-ADC) histogram. In true T_2-ADC histograms the separation of tissue-characterizing regions was less pronounced (Fig. 2); 2) DWI should be included if T_1- or T_2-weighted signal intensities (T_1w, T_2w SI) do not show clear abnormalities (in the hyperacute phase (8) or if T_2 or T_2w SI of ischemic regions are comparable to adjacent structures, e.g., CSF); 3) hemorrhagic regions with elevated T_1w SI can best be segmented by including T_1w images. True T_1-ADC histograms did not lead to a better segmentation.

Relative mean T_2w SI and mean ADC values obtained by a T_2w-ADC histogram analysis are summarized in Table 1. Decreased ADC values and increased T_2w SI were observed between day 1 and day 6 after the onset of ischemia. Relative mean ADC and T_2w SI were increased for patient 2 when examined 16 days, and patient 3 when examined 4 months, after stroke. The time after the ischemic event correlated with an increase of the relative mean T_2w SI (r = 0.87) and relative mean ADC values (r = 0.91). Data were also analyzed by segmenting ischemic and unaffected tissues interactively within the parameter images (Table 1). Comparing the histogram-based method with the image-

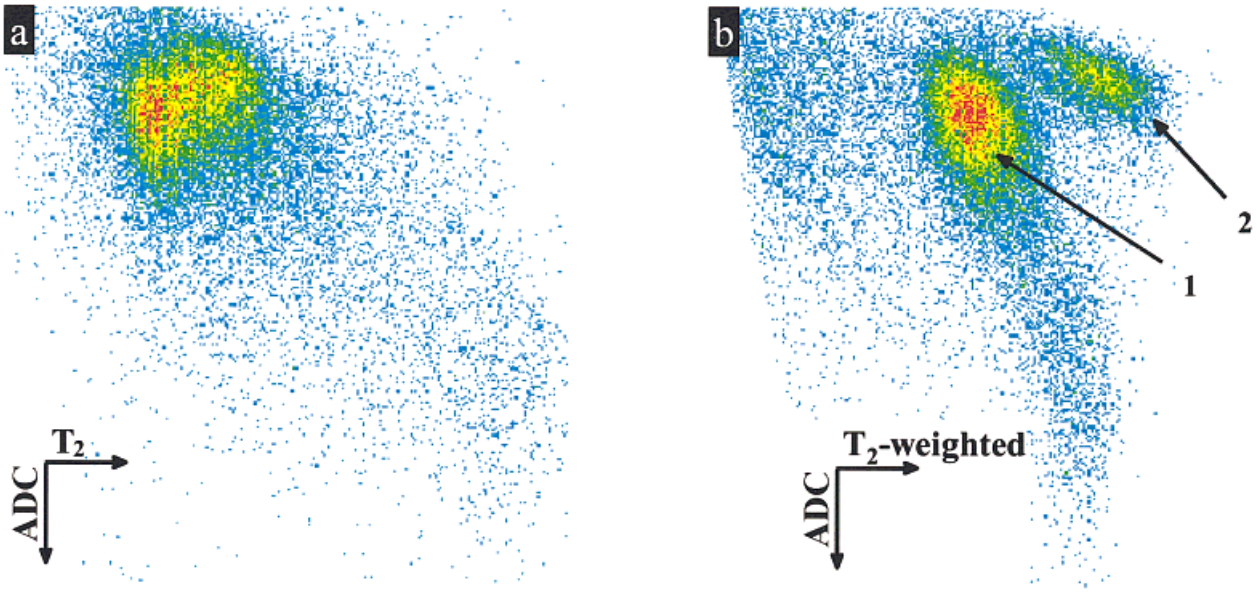

FIG. 2. Histogram-based analysis of a patient three days after the onset of an extended right hemispheric stroke. Histograms of quantitative T_2-ADC (**a**) and T_2-weighted-ADC values (**b**). Cluster 2 in b, which corresponds to the ischemic regions, is more clearly separated from cluster 1, which characterizes the unaffected tissue. ADC values are ordered ascending in negative *y*-direction, T_2 values, and T_2-weighted signals ascending in positive *x*-direction. T_2 values are scaled logarithmically in a. The frequency of the histogram cells is encoded blue for low and red for high frequency.

based method, no significant differences were found for the relative sizes of ischemic regions ($P = 0.679$), relative mean T_2w SI ($P = 0.189$), relative mean ADC values ($P = 0.68$), and for the total relative number of false-positive voxels ($P = 0.94$). However, significant differences were found by comparing the subclasses of false-positive voxels (see Table 1 for details): In the image-based segmentation, more voxels were classified as ischemic tissue but exhibited characteristics of unaffected brain parenchyma (mean of ratios [mR] of class IA = 0.039, mR of class IIA = 0.066; $P = 0.04$) or of partial volume effects (mR of class IB = 0.031, mR of class IIB = 0.091; $P = 0.01$). Using the histogram method, more voxels were classified as ischemic tissue but were located in adipose tissue or muscle (mR of class IC = 0.123, mR of class IIC = 0.034; $P = 0.028$).

DISCUSSION

The complex patterns of MR signals as a result of perfusion changes of tissues were analyzed in experimental and clinical studies: the decline of the ADC at normal T_2 in the hyperacute phase followed by a T_2 rise at a still reduced but slowly increasing ADC in the following days; potential reverse of the ADC decline after reperfusion, where reperfused regions may not match regions with decreased diffusion; and different behavior of T_2 and ADC in the chronic phase depending on tissue evolution (1,3–9,11–15,23,29). These complex processes may be analyzed either separately in each original image or in a unified approach by segmenting ROIs with similar parameter combinations in one histogram. Within this histogram correlations between parameters are immediately depicted by the shape, extension, and main axes of the clusters.

Nonischemic Tissue

The feature-based segmentation allowed the characterization of even geometrically complex, irregular or disconnected tissues, or of tissue zones with transition characteristics between different tissue types (e.g., CSF adjacent to GM). This is seen in Fig. 1, where quantitative parameter vectors were determined for GM by combining T_1 with T_2 and with ADC maps (Fig. 1). Partial volume effects and the direction-dependent ADC values in WM tracts were resolved (Fig. 1). More information about the direction dependence of the ADC could be obtained by tensor-imaging techniques (31). However, tensor-imaging with navigated spin echo DWI prolongs the examination procedure, which may be intolerable for patients in poor condition. Additionally, isotropic ADC maps lead to decreased image contrast, reducing the efficiency of the histogram analysis and resulting in a more difficult characterization of strongly anisotropic structures (e.g., the brain stem). In most cases pathologic regions can be differentiated from anisotropy effects by comparing contralateral unaffected structures.

ADC values are in good agreement with reported ADC values for GM of 850 ± 60 μm^2/sec (9) and 1000 ± 200 μm^2/sec (32). Reported ADC value ranges for WM were 450–850 μm^2/sec (9), between 220 ± 220 μm^2/sec and 1070 ± 60 μm^2/sec (33), and 700 ± 200 μm^2/sec (34) compared with the mean ROI value of 810 ± 270 μm^2/sec obtained by our analysis. CSF shows a wide distribution of ADC values: 2200 μm^2/sec (9), 2940 ± 50 μm^2/sec (33), and 3500 ± 700 μm^2/sec (34).

Only a few histogram-based results have been reported for quantitative relaxation times of human brain tissues at 1.5 T. Fletcher et al. (18) reported segmentation ranges for T_1 times between 1090–2150 msec (center: 1430 msec) for GM, 760–1080 msec (center: 893 msec) for WM, 800 msec–20 sec for CSF (no center specified), 950–1820 msec (center: 1333 msec) for muscle, and 200–750 msec (center: 417 msec) for adipose tissue. Segmentation ranges for T_2 times were 61–109 msec (center: 80 msec) for GM, 61–100 msec (center: 77 msec) for WM, 110–2000 msec for CSF (no

center specified); 20–67 msec (center: 52 msec) for muscle, and 53–94 msec (71 msec) for adipose tissue. Their results agree with our findings, except for their somewhat high T_1 of 1430 msec for GM compared to our result of 1070 msec and to other reported values of 870 msec and 921 msec (35,36).

Alfano et al. (19), reported only segmentation ranges for T_1 times of 800–2381 msec for GM, 465–794 msec for WM, $>$ 952 msec for CSF, $>$ 457 msec for muscle, and 392–454 msec for adipose tissue. Segmentation ranges for T_2 times were 58–119 msec for GM, 54–88 msec for WM, 125–2777 msec for CSF, 32–46 msec for muscle, and $>$ 32 msec for adipose tissue.

Ischemic Tissue

The advantage of quantitative tissue characterization using true T_1 and T_2 relaxation times was counteracted by the prolonged examination time, which prevented the acquisition of quantitative data for three patients in poor condition. Since true relaxation times did not provide a better segmentation than the corresponding T_1w and T_2w SI, their acquisition may be skipped if no exact relaxation times are required. Other intrinsic difficulties of analyzing human ischemic regions will be demonstrated by two typical cases.

The first case (Fig. 3) illustrates heterogeneous ischemic areas as well as the different influences of hemorrhagic transformations on relaxation times and ADC calculation. The patient was examined two days after the sudden onset of a left-sided visual and sensory hemineglect and hemiplegia caused by an occlusion of the right MCA. The symptoms did not improve over the next two weeks. The region exhibiting reduced signals in both the T_2w image (Fig. 3b, arrow) and the DWI (Fig. 3c) was interpreted as a beginning hemorrhagic transformation (37). Figure 4 displays representative color-encoded overlays of 2 different histogram-based segmentations. Inclusion of T_1w images (Fig. 3a) in the histogram allowed a better characterization of the hemorrhagic parts with elevated T_1w SI. Compared to the frontomedial part (Fig. 3b, arrow), the hemorrhagic region in the medial part of the segmented ischemic region (Fig. 4, arrow) exhibits T_2- and diffusion-weighted signals above noise level. The ADC values for this region are therefore more reliable than those in the frontomedial part.

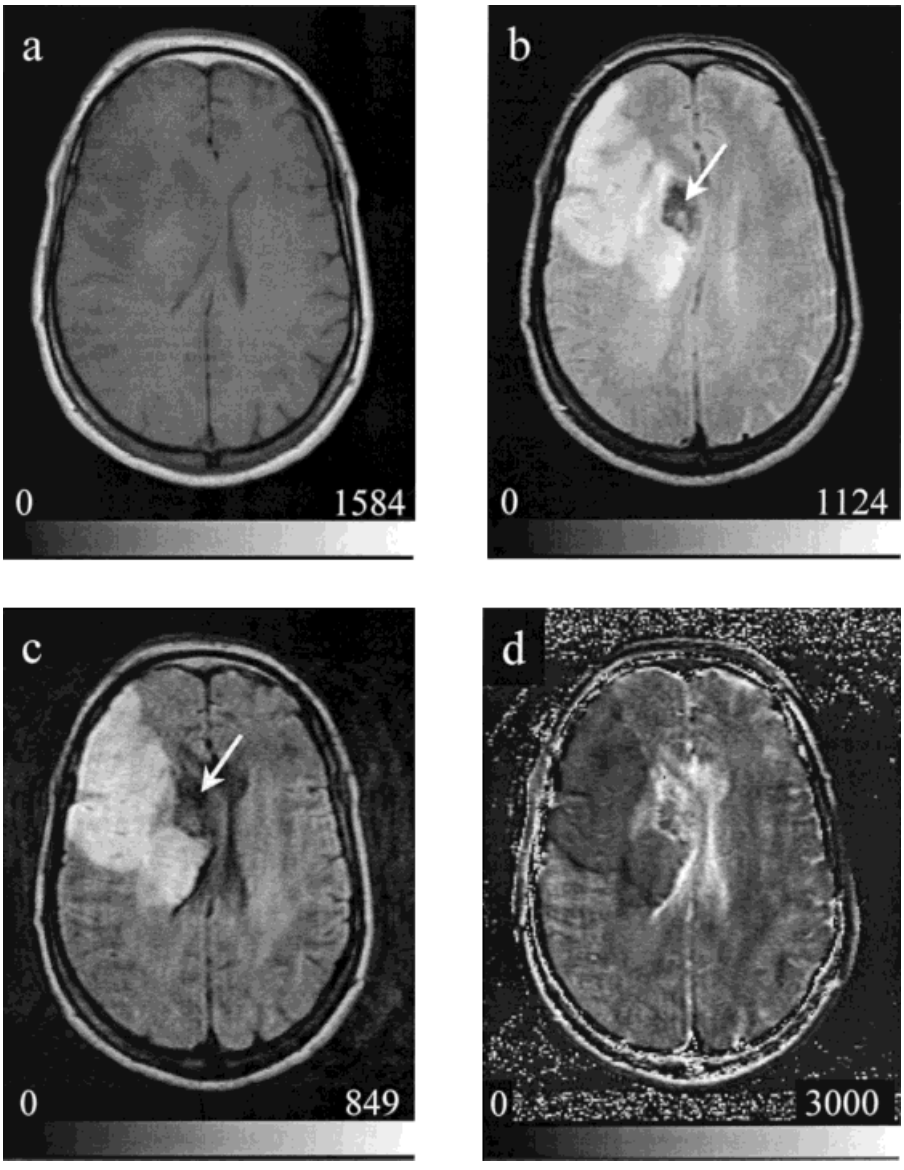

FIG. 3. T_1w image (**a**), T_2w image (**b**), DWI (**c**; *b*-factor = 529 sec/mm^2), and ADC map (**d**) of a patient 2 days after the onset of stroke (case 1). In the T_1w image, a lateral hypointense and a medial hyperintense zone can be differentiated whereas the main parts of the ischemic region are more clearly demarcated as hyperintense regions in the diffusion-weighted image (**c**) with already elevated T_2w SI (**b**). Corresponding ADC values are decreased (**d**). A region with strongly reduced T_2w SI (**b**, arrow), interpreted as tissue with a beginning hemorrhagic transformation (38), remained hypointense after additional diffusion weighting (**c**). The reduced signal of CSF spaces in the DWI is because of the high mobility of water protons (**d**).

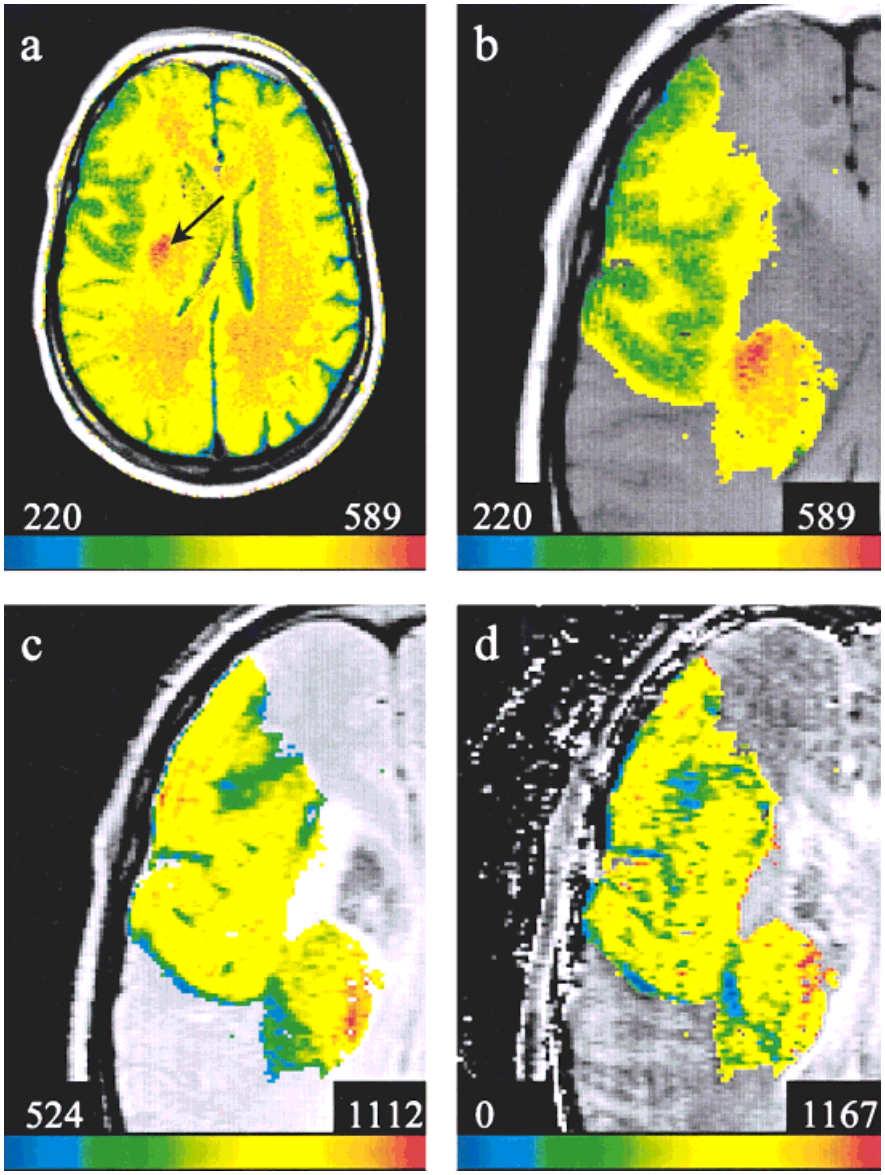

FIG. 4. Representative results of an interactive 4D histogram-based analysis of the data presented in Fig. 3 using the T_1w image (3a), the T_2w image (3b), the DWI (3c), as well as the ADC map (3d). The values of image parameters are color-encoded according to their segmentation ranges (shown in the lower bar; arbitrary units [a.u.] for signal intensities [SI] and μm^2/sec for ADC). Here both the color-encoded overlays and the original parameter images are displayed. **a:** T_1w SI for unaffected and ischemic brain tissues (not shown are the overlays of T_2w SI [segmentation range 291–1124 a.u.], of the diffusion-weighted signals [s.r. 42–849 a.u.] and of the ADC values [s.r. 0–3493 μm^2/sec]). The color-encoded T_1w SI allow the differentiation of GM, WM, a lateral part of the ischemic region with reduced T_1w SI indicating edema, and a hyperintense hemorrhagic region within the medial part of the ischemic region (arrow). **b–d:** The segmentation of tissue that is hyperintense in the DWI (compare Fig. 3c) is achieved by changing the segmentation ranges. Original and color-encoded overlays of the magnified segmented parts of T_1w SI (**b**), T_2w SI (**c**), and ADC values (**d**) visualize in more detail the spatial heterogeneity of the parameters. In contrast to the frontomedial region with T_2 signal loss (compare Fig. 3b and c) the hemorrhagic region (**a**, arrow) in the medial part of the segmented ischemic region still has T_2w and diffusion-weighted SI well above noise level, leading to more reliable ADC values. Within the segmented overlay (**d**) local values of the ADC range from subnormal (blue and green) to above normal values (red). The mean ADC value of the segmented region is 60% that of mean ADC value of unaffected brain parenchyma. (Not shown is the overlay of diffusion-weighted SI with a segmentation range of 461–788 a.u.)

Case 2 illustrates lesions with different parameter combinations (Fig. 5) as well as the determination of ADC values of small lesions adjacent to structures with intense T_2 signals (Fig. 6). The patient suffered from a sudden dysarthria and a right-sided weakness (face and arm) six days before examination, his condition deteriorating with an aphasia one day before examination. The DWI showed two hyperintense lesions with different combinations of T_2w SI and ADC values (see figure caption for details). The partial overlap of the 1D ADC distributions of unaffected and ischemic tissues was resolved using a T_2w-ADC histogram. Additional small cortical ischemic lesions could not be localized unambiguously in the T_2w image due to the intense T_2 signal of the adjacent CSF (Fig. 6a), whereas they were well demarcated in the DWI (Fig. 6b). The spatial distribution of the ADC is therefore more reliably deter-

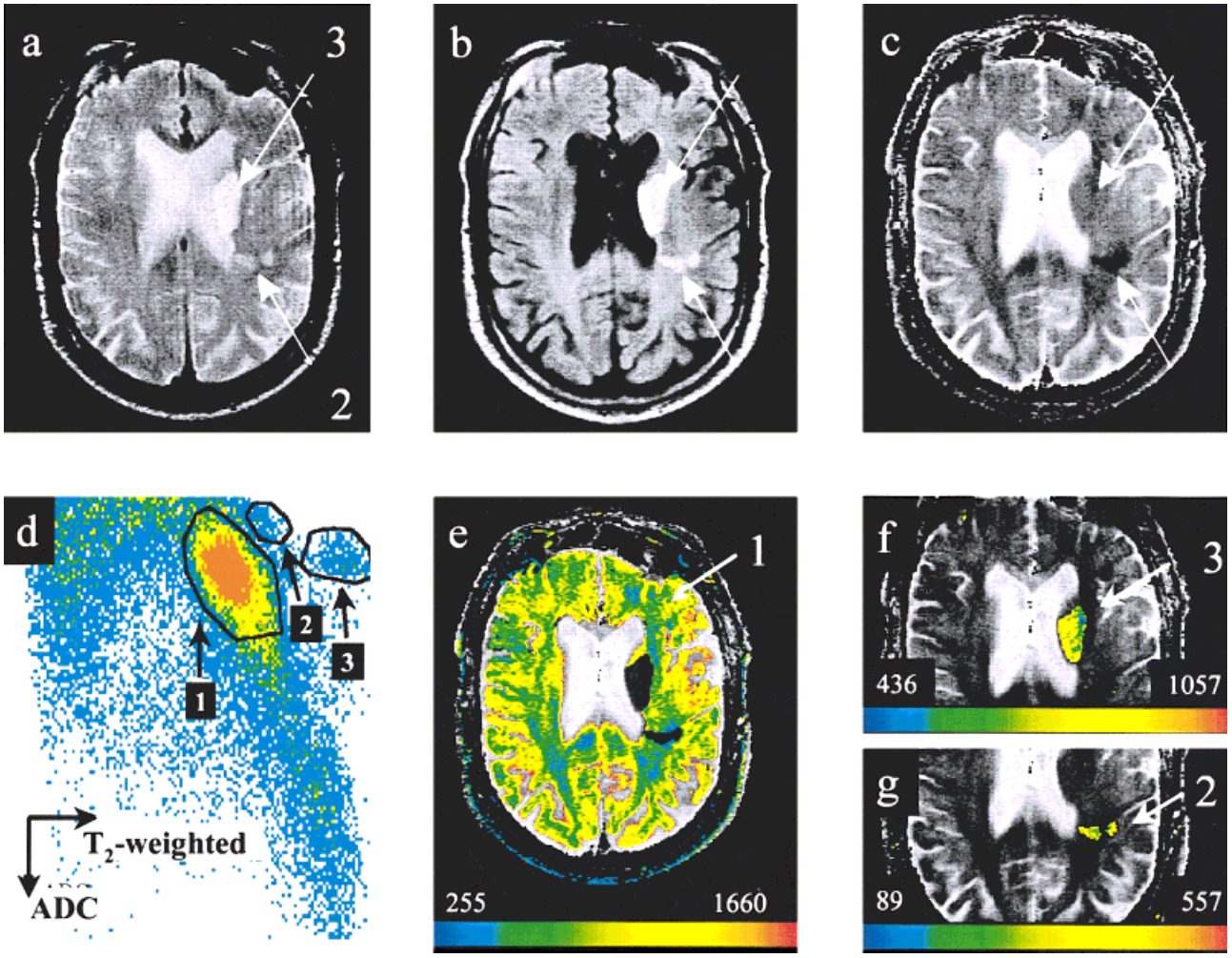

FIG. 5. T_2w image (**a**), DWI (**b**; *b*-factor = 529 sec/mm^2), and ADC map (**c**) of a patient 6 days after the onset of a progressive stroke (case 2). **d:** Histogram of T_2w SI and ADC values. ADC map with color-encoded overlays corresponding to region of interest (ROI) 1 (**e**), ROI 2 (**g**), and ROI 3 (**f**) of the histogram. ROI 1 characterizes the unaffected GM and WM except voxels with partial volume effects between GM and CSF. ROI 2 characterizes an ischemic region with slightly elevated T_2w SI values but strongly decreased ADC values (mean ROI ADC 37% that of normal). ROI 3 characterizes the ischemic area with strongly elevated T_2w SI values but with only a slightly decreased ADC mean value (85% that of normal).

mined using a DWI-ADC histogram. Fig. 6b also illustrates the high spatial resolution and the undistorted geometry of navigated spin-echo DWI, which allows the exact localization of even small cortical ischemic regions.

To determine the parameter vectors of tissues using image-based segmentation rather than the histogram method required the segmentation of a pathologic region within one parameter image, a subsequent transfer of this ROI to other images, and an analysis of a possible mismatch between pathologic structures in different images. Applying both methods, no significant differences were found for lesion sizes, parameter mean values, and total number of false-positive voxels (Table 1). A further analysis revealed, however, that the image-based segmentation of ischemic regions with increased partial volume effects and complex anatomical structures was often tedious (patients 1–4, see performance). A differentiation between lesion, parenchyma, and CSF was difficult for heterogeneous ischemic regions. Consequently, the relative number of voxels with characteristics of unaffected brain parenchyma or partial volume effects (IIA, IIB) was higher than found in the histogram method (IA, IB). In the histogram method, parenchyma and partial volume parts were well separated (Fig. 1) except in images with reduced signal-to-noise ratio (SNR; patients 1 and 3). Voxels with low ADC values, reflecting the influence of direction-dependent ADC values or noise, are usually fewer in number in the image ROIs than in histogram-segmented regions (IIC).

The histogram-based segmentation led to less reliable results for tissues with overlapping or scattered parameters, for instance parts of muscle or adipose tissue with broadly distributed and subnormal ADC values (IC). Their relative number is greater in small lesions with a strongly decreased mean ADC (patient 9), in images with reduced SNR (patient 1), or in images displaying more muscle or adipose tissue (patient 3). This effect may be reduced by including fat-suppressed or dark-fluid images into the histogram-analysis.

Histogram Analysis

The task of characterizing tissue parameters of pathologic tissues as increased, decreased, or normal with respect to parameters of unaffected tissue depends on the strategy of the histogram analysis: Welch et al. determined thresholds

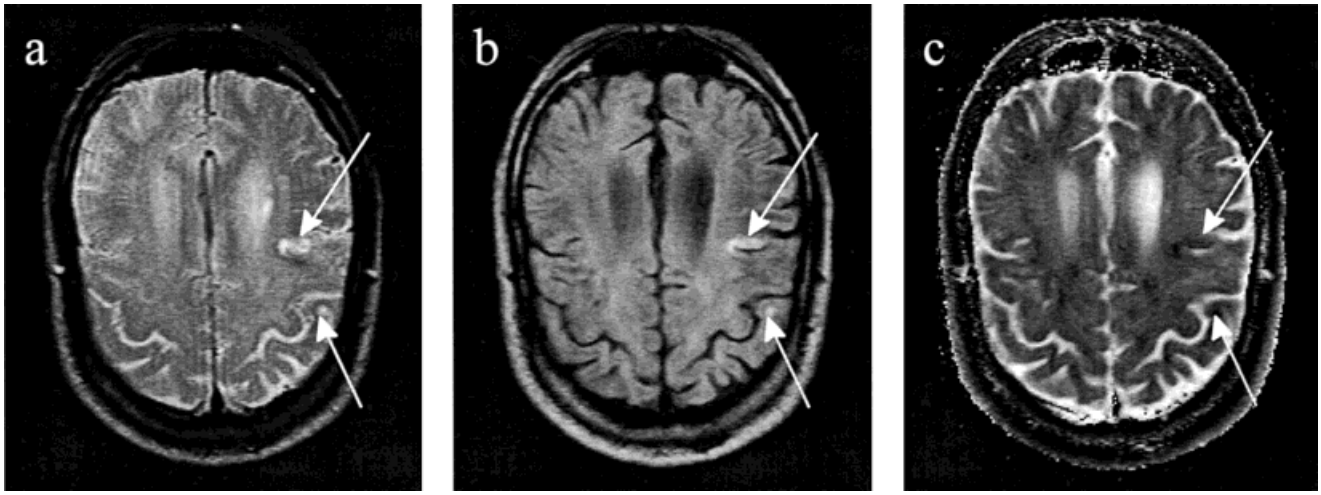

FIG. 6. T_2w image (**a**), DWI (**b**, *b*-factor = 529 sec/mm^2), and ADC map (**c**) at a second slice position of the patient shown in Fig. 5. In **a**, the lesions (arrows) can hardly be differentiated from adjacent structures with high T_2w SI intensities (CSF). The high spatial resolution of navigated spin-echo DWI allows a clear differentiation of even small ischemic regions (**b**, arrow) exhibiting a reduced mean ADC value of about 60% that of normal values.

for normal ADC values and T_2w SI of unaffected tissue (5) and divided the remaining histogram into rectangular regions representing combinations of decreased, normal, or increased ADC-T_2w SI. Corresponding parameter combinations were correlated to different tissue signatures (5). Applying this method to the histogram in Fig. 2b, cluster 2 would probably be described as tissue with normal ADC and elevated T_2w SI. However, the overall ADC distribution and the mean ADC of this cluster is clearly shifted toward lower values compared to the cluster for unaffected brain parenchyma. Connected clusters may also be localized in more than one histogram region or within regions ascribed to normal values (e.g., cluster 2 in Fig. 6). Among other reasons, this different tissue ''labeling'' may be one of the reasons why Welch et al. observed elevated ADC values at an earlier time than other groups did (6,7). While segmenting connected ROIs, we found subnormal mean ADC values during the first week after the onset of ischemia (Table 1). In later stages (16 days, 4 months), mean ADC values were supranormal, which coincides with the results of other groups (4,8). T_2 values were always supranormal. Since both parameters exhibited increasing values for longer time periods after the ischemia, progressive strokes may be characterized by lesions with different combinations of mean ADC and T_2. This might explain the different parameter combinations of the ischemic regions observed in case 2. However, comparing ischemic and unaffected brain tissue ROIs, some ischemic tissue parts exhibited ADC values that were increased relative to unaffected tissue parts while the overall ischemic region exhibited a still decreased mean ADC. Whether locally increased ADC values are due to anisotropy effects or whether parts of ischemic tissues exhibit increased ADC values at early points in time (5) has yet to be investigated.

CONCLUSION

The combined determination of ADC, true relaxation times, DWI, T_1w SI, and T_2w SI using a histogram-based data analysis compensates for strongly fluctuating parameters such as ADC values. This, together with the color-encoded representation of the spatial distribution of the parameter values, allows a characterization of heterogeneous healthy and ischemic tissue structures, which is the prerequisite for investigating parameter combinations as predictive values for tissue evolution toward recovery or necrosis. Combined normal values of true relaxation times and ADC were determined for healthy brain tissues. Navigated spin-echo DWI provided the necessary spatial resolution without geometric distortions for the exact localization of small cortical infarcts. To characterize the ADC distribution of ischemic tissue in the hyperacute phase (< 6h) or adjacent to hyperintense T_2 signals, DWI should be combined with ADC maps. In later stages combined ADC maps and T_2w images deliver the best results with regard to examination duration and segmentation of pathologic tissue. Influences of hemorrhagic transformations have to be analyzed by including T_1w images. Reduced mean ADC values and increased T_2w SI were found between day 1 and day 6 after the onset of ischemia.

Compared with image-based ROI methods, the histogram-based analysis relies on characteristic parameter combinations and is therefore better suited for characterizing irregular, scattered, or heterogeneous ischemic regions. The method is less reliable for tissues with overlapping or broadly distributed parameter combinations. Image-based methods are better suited for connected structures with homogeneous characteristics and reduced partial volume effects (e.g., ischemic regions in basal ganglia). Both methods are complementary to some degree, since the characteristics of image-based segmented voxels are easily verified by a projection onto the corresponding histogram. Extending the histogram analysis to include perfusion imaging and additional metabolic information (12,15,38) will increase its potential to describe ischemic zones with different metabolic characteristics, such as tissue at risk. This may help to more precisely evaluate new therapeutic strategies.

ACKNOWLEDGMENTS

This project was supported in part by the DFG (Deutsche Forschungsgemeinschaft). The authors thank Georg Haupt and Klaus Haarbeck for implementing the software system for the image analysis and Jean Pietrowicz for proofreading the manuscript.

REFERENCES

1. Moseley ME, Cohen Y, Mintorovitch J, Chileuitt L, Shimizu H, Kucharczyk J, Wendland MF, Weinstein PR. Early detection of regional cerebral ischemia in cats: comparison of diffusion-weighted and T_2-weighted MRI and spectroscopy. Magn Reson Med 1990;14:330–346.
2. Busch E, Krüger K, Allegrini PR, Kerskens C, Gyngell ML, Hoehn-Berlage M, Hossmann KA. Reperfusion after thromboembolic therapy of embolic stroke in Rat. Magnetic Resonance and Biochemical Imaging. J Cereb Blood Flow Metab 1998;18:407–418.
3. Moseley ME, Butts K, Yenari MA, Marks M, de Crespigny A. Clinical aspects of DWI. NMR Biomed 1995;8:387–396.
4. Marks MP, de Crespigny A, Lentz D, Denzmann DR, Albers GW, Moseley ME. Acute and chronic stroke: navigated spin-echo diffusion-weighted MR Imaging. Radiology 1996;199:403–408.
5. Welch KMA, Windham J, Knight RA, Nagesh V, Hugg JW, Jacobs M, Peck D, Booker P, Dereski MO, Levine SR. A model to predict the histopathology of human stroke using diffusion and T2-weighted magnetic resonance imaging. Stroke 1995;26:1983–1989.
6. Warach S, Moseley M, Sorensen GA, Koroshetz W. Time course of diffusion imaging abnormalities in human stroke. Note to the editor. Stroke 1996;27:1254–1255.
7. Welch KMA, Levine SR, Chopp M, Knight RA, D'Olhaberriague L, Boska MD, Nagesh V, Windham JP, Peck D. Response to: time course of diffusion imaging abnormalities in human stroke. Note to the editor. Stroke 1996;27:1255–1256.
8. Warach S, Gaa J, Siewert B, Wielopolski P, Edelman RR. Acute human stroke studied by whole brain echo planar diffusion-weighted magnetic resonance imaging. Ann Neuro 1995;37:231–241.
9. de Crespigny AJ, Marks MP, Enzmann DR, Moseley ME. Navigated diffusion imaging of normal and ischemic human brain. Magn Reson Med 1995;33:720–728.
10. Conturo TE, McKinstry RC, Aronovitz JA, Neil J. Diffusion MRI: precision, accuracy and flow effects. NMR Biomed 1995;8:307–332.
11. Röther J, de Crespigny A, D'Arcueil H, Iwai K, Moseley M. Recovery of apparent diffusion coefficient after ischemia-induced spreading depression relates to cerebral perfusion gradient. Stroke 1996;27:980–987.
12. Kohno K, Hoehn-Berlage M, Mies G, Back T, Hossmann KA. Relationship between diffusion-weighted MR-images, cerebral blood flow, and energy state in experimental brain infarction. Magn Reson Imaging 1995;13:73–80.
13. Hoehn-Berlage M, Eis M, Back T, Kohno K, Yamashita K. Changes of relaxation times (T_1, T_2) and apparent diffusion coefficient after permanent middle cerebral artery occlusion in the rat: temporal evolution, regional extent, and comparison with histology. Magn Reson Med 1995;34:824–834.
14. Hossmann KA, Hoehn-Berlage M. Diffusion and perfusion MR imaging of cerebral ischemia. Cerebrovascular and Brain Metabolism Reviews 1995;7:187–217.
15. Warach S, Dashe JF, Edelman RR. Clinical outcome in ischemic stroke predicted by early diffusion-weighted and perfusion magnetic resonance imaging: a preliminary analysis. J Cereb Blood Flow Metab 1996;16:53–59.
16. Eis M, Hoehn-Berlage M. A time-efficient method for combined T_1- and T_2- measurement in magnetic resonance imaging: evaluation for multiparameter tissue characterization. MAGMA 1994;2:79–89.
17. Tolxdorff T, Handels H, Bohndorf K. Advantages of multi-exponential T_2-analysis. In: Higer HP, Bielke G, editors. Tissue characterizing in MR-imaging. Berlin: Springer; 1990. p 75–80.
18. Fletcher LM, Barsotti JB, Hornak JP. A multispectral analysis of brain tissues. Magn Reson Med 1993;29:623–630.
19. Alfano B, Brunetti A, Covelli EM, Quarantelli M, Panico MR, Ciarmiello A, Salvatore M. Unsupervised, automated segmentation of the normal brain using a multispectral relaxometric magnetic resonance approach. Magn Reson Med 1997;37:84–93.
20. Eis M, Handels H, Hoehn-Berlage M, Lwilmes LJ, Ernestus RI, Kloiber O, Tolxdorff T, Hossmann KA. Fully automatic tissue characterization in rat brain at 4.7 Tesla. In: Proc SMRM, 10th Annual Scientific Meeting, 1991. p 1214.
21. Hoehn-Berlage M, Tolxdorff T, Bockhorst K, Okada Y, Ernestus RI. In vivo NMR T_2 relaxation of experimental brain tumors in the cat: a multiparameter tissue characterization. Magn Reson Imaging 1992;10: 935–947.
22. Braun J, Bernarding J, Haupt G, Hohmann J, Haarbeck K, Tolxdorff T, Wolf KJ. Using automated tissue characterization in qualitative and quantitative MR imaging. In: Proc ISMRM, 5th Scientific Meeting, Vancouver, 1997. p 48.
23. Nagesh V, Welch KMA, Windham J, Patel S, Levine SR, Hearshen D, Peck D, Robbins K, D'Olhaberriage L, Soltanian-Zadeh H, Boska MD. Time course of ADC_w changes in ischemic stroke: beyond the human eye! Stroke 1998;29:1778–1782.
24. Anderson W, Gore JC. Analysis and correction of motion artifacts in diffusion weighted imaging. Magn Reson Med 1994;32:379–387.
25. Stejskal EO, Tanner JE. Spin diffusion measurements: spin echoes in the presence of a time-dependent field gradient. J Chem Physics 1965;42: 228–292.
26. Ordidge RJ, Helpern JA, Qing ZX, Knight RA, Nagesh V. Correction of motional artifacts in diffusion-weighted MR images using navigator echoes. Magn Reson Imaging 1994;12:455–460.
27. Woods RP, Grafton ST, Holmes CJ, Cherry SR, Mazziotta JC. Automated image registration: I. General methods and intrasubject, intramodality validation. J Comput Assist Tomogr 1998;22:141–154.
28. Conturo TE, Beth AH, Ahrensdorf RF, Price RR. Simplified mathematical description of longitudinal recovery in multiple-echo sequences, Magn Reson Med 1990;4:282–288.
29. Bernarding J, Braun J, Hohmann J, Kurth R, Wolf KJ, Tolxdorff T. Time course of the diffusion coefficient and relaxation times in human cerebral infarcts. MAGMA 1997;5(Suppl):69.
30. Wharton SA. Generalized histogram clustering scheme for multidimensional image data. Pattern Recognition 1983;16:193–199.
31. Pierpaoli C, Jezzard P, Basser PJ, Barnett A. Quantitative diffusion tensor imaging of the human brain. In: Proc ESMRMB, 13th Annual Meeting, 1996. p 70.
32. Chien D, Buxton RB, Kwong KK, Brady TJ, Rosen BR. MR diffusion imaging the human brain. J Comput Assist Tomogr 1990;14:514–520.
33. LeBihan D, Turner R, Douek P, Patronas N. Diffusion MR imaging: clinical applications. Am J Radiol 1992;159:591–599.
34. Chien D, Kwong K, Gress DR, Buonanno FS, Buxton RB, B. Rosen BR. MR diffusion imaging of cerebral infarction in humans. Am J Neuroradiology 1992;13:1097–1102.
35. Bottomley PA, Foster TH, Raymond EA, Pfeifer LM. A review of normal tissue hydrogen NMR relaxation times and relaxation mechanisms from 1—100 MHz: dependence on tissue types, NMR frequency, temperature, species, excision, and age. Medical Physics 1984;11:425–48.
36. Wehrli FW. Principles of magnetic resonance. In: Stark DE, Bradley WG, editors. Magnetic resonance imaging. 2nd ed. St. Louis: Mosby Year Book Inc.; 1992. p 3–20.
37. Bradley WG. Hemorrhage and brain iron. In: Stark DE, Bradley WG, editors. Magnetic resonance imaging. 2nd ed. St. Louis: Mosby Year Book Inc.; 1992. p 721–768.
38. Back T, Hoehn-Berlage M, Kohno K, Hossmann KA. Diffusion nuclear magnetic resonance imaging in experimental stroke. Stroke 1994;25:494–500.